Available online at www.sciencedirect.com
ScienceDirect
Journal of Sound and Vibration 311 (2008) 1228–1248
JOURNAL OF SOUND AND VIBRATION
www.elsevier.com/locate/jsvi

Efficiency of targeted energy transfers in coupled nonlinear oscillators associated with 1:1 resonance captures: Part I

D. Dane Quinn[a,*], Oleg Gendelman[b], Gaetan Kerschen[c], Themistoklis P. Sapsis[d,f], Lawrence A. Bergman[e], Alexander F. Vakakis[f,g]

[a]*Department of Mechanical Engineering, The University of Akron, Akron, OH 44325-3903, USA*
[b]*Faculty of Mechanical Engineering, Technion—Israel Institute of Technology, Technion City, Haifa 32000, Israel*
[c]*Aerospace and Mechanical Engineering Department (LTAS), Université de Liège, Liège, Belgium*
[d]*Department of Mechanical Engineering, Massachusetts Institute of Technology, Cambridge, MA 02139, USA*
[e]*Department of Aerospace Engineering, University of Illinois at Urbana-Champaign, 104 S. Wright St., 321E Talbot Lab, MC-236, Urbana, IL 61801, USA*
[f]*Division of Mechanics, National Technical University of Athens, P.O. Box 64042, GR-157 10 Zografos, Athens, Greece*
[g]*Department of Mechanical Science and Engineering (Adjunct), University of Illinois at Urbana-Champaign, 1206 West Green St., Urbana, IL 61801, USA*

Received 1 November 2006; received in revised form 5 October 2007; accepted 8 October 2007
Available online 26 November 2007

Abstract

We study targeted energy transfers and nonlinear transitions in the damped dynamics of a two degree-of-freedom system of coupled oscillators (a linear oscillator with a lightweight, essentially nonlinear, ungrounded attachment), caused by 1:1 resonance captures of the dynamics. Part I of this work deals with the underlying structure of the Hamiltonian dynamics of the system, and demonstrates that, for sufficiently small values of viscous damping, the damped transitions are strongly influenced by the underlying topological structure of periodic and quasiperiodic orbits of the corresponding Hamiltonian system. Focusing exclusively on 1:1 resonance captures in the system, it is shown that the topology of these damped transitions affect drastically the efficiency of passive energy transfer from the linear system to the nonlinear attachment. Then, a detailed computational study of the different types of nonlinear transitions that occur in the weakly damped system is presented, together with an analytical treatment of the nonlinear stability of certain families of periodic solutions of the underlying Hamiltonian system that strongly influence the said transitions. As a result of these studies, conditions on the system and forcing parameters that lead to effective or even optimal energy transfer from the linear system to the nonlinear attachment are determined. In Part II of this work, direct analytical treatment of the governing strongly nonlinear damped equations of motion is performed, in order to analytically model the dynamics in the region of optimal energy transfer, and to determine the characteristic time scales of the dynamics that influence the capacity of the nonlinear attachment to passively absorb and locally dissipate broadband energy from the linear oscillator.

*Corresponding author. Tel.: +1 330 972 6302; fax: +1 330 972 6027.
E-mail address: quinn@uakron.edu (D.D. Quinn).

0022-460X/$ - see front matter © 2007 Elsevier Ltd. All rights reserved.
doi:10.1016/j.jsv.2007.10.026

1. Introduction

The aim of this work is to study the complex transitions in the dynamics and targeted energy transfers associated with the attraction of the transient dynamics of a two degrees- of- freedom (dof) strongly nonlinear system into 1:1 resonance capture [1,2]. In particular, the transient dynamics of a linear damped oscillator (labeled as primary system) with an essentially nonlinear, damped, lightweight attachment are investigated. The complexity of the problem dictates an extensive series of numerical simulations, together with the development of methodologies capable of analytically modeling both qualitatively and quantitatively the transient, strongly nonlinear transitions.

As reported in earlier works [3,4] the two degrees of freedom system under consideration possesses surprisingly complex dynamics. Moreover, at certain ranges of parameters and initial conditions passive targeted energy transfer passive targeted energy transfer is possible, whereby vibration energy initially localized in the linear oscillator (LO) gets passively transferred to the lightweight attachment in a one-way irreversible fashion. Interesting features of passive targeted energy transfer in this system are the ability of the attachment (labeled nonlinear energy sink—nonlinear energy sink) to irreversibly absorb broadband vibration energy, and, in cases of multi-degree-of-freedom primary structures, to engage in a sequential resonance captures with a set of modes of the primary structure, passively absorbing energy from each before engaging the next [5]. In essence, the nonlinear energy sink acts as a passive, adaptive and broadband boundary controller. As explained in the mentioned references, what enables the local nonlinear energy sink attachment to affect the global dynamics of the primary structure is its lack of a preferential resonance frequency (since it possesses an essentially nonlinear—nonlinearizable—stiffness nonlinearity), giving rise to degenerate, high-codimension bifurcations of the underlying Hamiltonian dynamics. In recent studies passive targeted energy transfer has been experimentally shown to exist and to be robust to small variations of parameters and initial conditions [6].

Previous works examined targeted energy transfer in systems of coupled nonlinear oscillators through energy exchanges between donor and acceptor discrete breathers due to nonlinear resonance [7–9]. In Ref. [10] resonant interactions between monochromatic electromagnetic waves and charged particles were studied, leading to chaotization of particles and transport in phase space. In Ref. [11] the processes governing energy exchange between coupled Klein–Gordon oscillators were analyzed; the same weakly coupled system was studied in Ref. [12], and it was shown that, under appropriate tuning, total energy transfer can be achieved for coupling above a critical threshold. In related work, localization of modes in a periodic chain with a local nonlinear disorder was analyzed [13]; transfer of energy between widely spaced modes in harmonically forced beams was analytically and experimentally studied [14]; and a nonlinear dynamic absorber designed for a nonlinear primary system was analyzed [15].

In Ref. [4] it was shown that there are (at least) three distinct mechanisms for passive targeted energy transfer in the two-degree-of-freedom system under consideration herein: namely, fundamental passive targeted energy transfer, subharmonic passive targeted energy transfer, and passive targeted energy transfer through nonlinear beats followed by 1:1 resonance capture. The latter mechanism is the most efficient for passive targeted energy transfer, as it permits a significant percentage of the vibration energy of the primary system to be transferred and then locally dissipated by the nonlinear energy sink. It is the principal aim of the current work to study in detail the complex nonlinear transitions associated with this passive targeted energy transfer mechanism and to determine the conditions for strong (or even optimal) passive targeted energy transfer in the two-degree-of-freedom system.

The first section of this work deals with the underlying structure of the Hamiltonian dynamics of the system and demonstrates that, for sufficiently small values of viscous damping, the damped transitions are strongly influenced by the underlying periodic and quasiperiodic orbits of the corresponding Hamiltonian system. Then, a detailed computational study of the different types of nonlinear transitions that occur in the weakly damped system is presented, together with an analytical treatment of the nonlinear stability of certain families of periodic solutions of the underlying Hamiltonian system that strongly influence the said transitions. In a companion paper, the second part of this work will be reported, focusing on direct analytical treatment of the governing strongly nonlinear equations of motions, theoretical modeling, and interpretation of the computational results.

Consider the following two degrees- of- freedom nonlinear system of coupled oscillators:

$$\ddot{y}_1 + 2\varepsilon\zeta_1\dot{y}_1 + 2\varepsilon\zeta_2(\dot{y}_1 - \dot{y}_2) + y_1 + \tfrac{4}{3}\varepsilon\alpha(y_1 - y_2)^3 = 0, \tag{1a}$$

$$\varepsilon\ddot{y}_2 + 2\varepsilon\zeta_2(\dot{y}_2 - \dot{y}_1) + \tfrac{4}{3}\varepsilon\alpha(y_2 - y_1)^3 = 0, \tag{1b}$$

viewed as a LO, described by y_1, coupled to a nonlinear energy sink whose response is measured by y_2, as illustrated in Fig. 1. This system, with $\zeta_1 = 0$, has also been the subject of the recent study by Manevitch, Musienko and Lamarqu [16].

In the absence of damping the total energy $E(t)$ in the system is conserved and given as $E(t) = E_1(t) + E_2(t)$, where

$$E_1(t) = \frac{\dot{y}_1^2(t)}{2} + \frac{y_1^2(t)}{2}, \tag{2a}$$

$$E_2(t) = \varepsilon\frac{\dot{y}_2^2(t)}{2} + \frac{\varepsilon\alpha}{3}(y_1(t) - y_2(t))^4. \tag{2b}$$

The quantity $E_1(t)$ can be interpreted as the energy in the LO, while $E_2(t)$ then represents the energy associated with the attachment. The energy in each component can be scaled by the total initial energy in the system, so that $h_i(t) \equiv E_i(t)/E(0)$. Finally, the instantaneous fraction of the total energy in each component is identified as $\hat{h}_i(t) \equiv E_i(t)/E(t)$.

With direct impulsive forcing of the primary system, i.e., $\dot{y}_1(0) = Y \neq 0$, $y_1(0) = y_2(0) = 0$, $\dot{y}_2(0) = 0$, the possibility of passively transferring a significant fraction of the imparted energy to the nonlinear energy sink, where it is coincidentally localized and dissipated, is examined. As an illustrative example, the response of Eqs. (1a) is computed with $\alpha = 1$, $\varepsilon = 0.05$, $\zeta_1 = 0.00$, $\zeta_2 = 0.10$ for an intermediate level of initial energy, $Y = 0.75$. As seen in Fig. 2, the response of the system can be characterized by three different regimes of motion. In the first interval, seen for $t > 10$ in this simulation, a fraction of the energy, initially localized to the LO, is rapidly transferred to the nonlinear energy sink. This is followed by a slow decay of the total energy in the system characterized by large amplitude response of both the nonlinear energy sink as well as the LO, exhibited here for $10 < t < 55$. In addition, in this interval the energy is slowly localized to the nonlinear energy sink as the energy decays. Finally, in the final regime of the motion for $t > 55$ the energy is again transferred back to the LO.

The response of the system is strongly dependent on the initial energy in the system. Fig. 3 depicts the system response at low- ($Y = 0.375$), moderate- ($Y = 0.50$) and high-energy ($Y = 1.00$) levels, together with the corresponding scaled energy in the system. Clearly, there are qualitative changes in the response of the system as the initial energy level increases. In the low-energy regime, no interesting energy transfer occurs from the LO to the nonlinear energy sink, and the response remains localized to the LO. As discussed in Refs. [3,4], significant targeted energy transfer takes place only above a well-defined critical threshold of input energy. Efficient passive targeted energy transfer to the nonlinear energy sink is triggered through the initial energy transfer noted above for $Y = 0.75$ in the moderate-energy regime (Figs. 3c, d). Gendelman, Kerschen, Vakakis, Bergman and McFarland [17] discuss the existence of impulsive periodic orbits in the underlying Hamiltonian system that play the role of bridging orbits and channel a significant portion of the energy initially localized in the LO to the nonlinear energy sink at a relatively fast time scale. As the initial energy is further increased (Figs. 3e, f), the initial triggering of the passive targeted energy transfer still occurs, but its effect on the overall energy dissipation in the system is diminished. As illustrated in Fig. 3, the nonlinear energy sink is most effective for an intermediate level of energy.

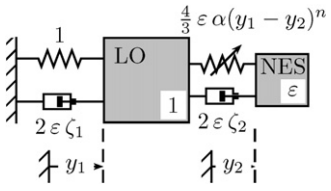

Fig. 1. Single degree-of-freedom oscillator coupled to an nonlinear energy sink (nondimensionalized).

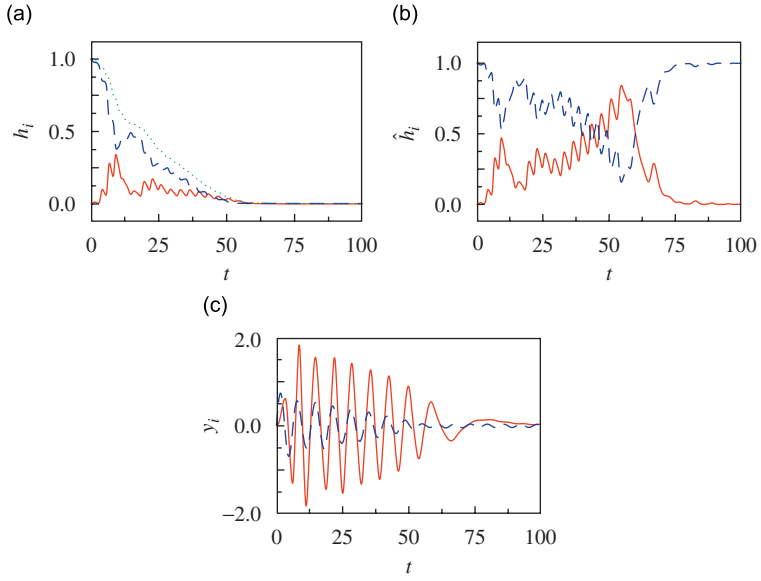

Fig. 2. Numerical simulations of Eq. (1), nonlinear energy sink: solid line, LO: dashed line ($Y = 0.75$, $\alpha = 1$, $\varepsilon = 0.05$, $\zeta_1 = 0.00$, $\zeta_2 = 0.10$); (a) h_1, h_2, $h_1 + h_2$: dashed line (b) $\hat{h}_1$, $\hat{h}_2$, (c) y_1, y_2.

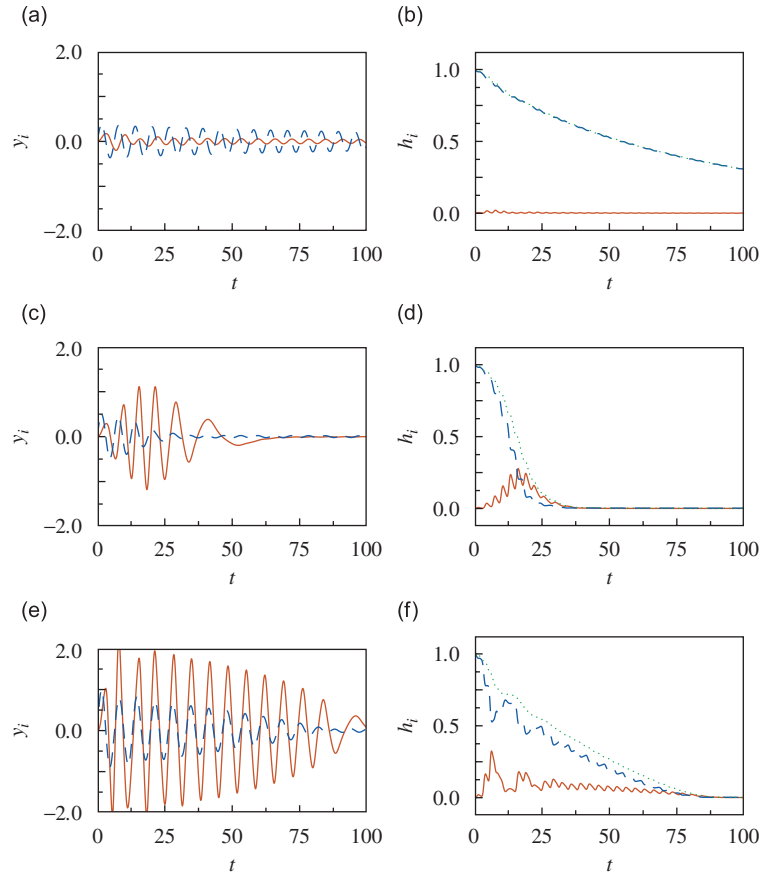

Fig. 3. Damped numerical simulations, nonlinear energy sink: solid line, LO: dashed line; left column: time series; right column: instantaneous scaled energy in each component ($\alpha = 1$, $\varepsilon = 0.05$, $\zeta_1 = 0.00$, $\zeta_2 = 0.10$); (a, b) low-energy $Y = 0.375$, (c, d) moderate-energy $Y = 0.50$, and (e, f) high-energy $Y = 1.00$. The dotted line in (b), (d), and (f) is the total scaled energy.

Indeed, these different regimes in the response are clearly seen in the instantaneous fraction of the energy in each component, $\hat{h}_i(t)$, shown in Fig. 4. For the low-energy regime the energy remains localized in the LO and passive targeted energy transfer does not occur. As the initial impulse is increased, seen in Fig. 4b, a significant fraction of the energy is transferred to the nonlinear energy sink, which is then able to effectively dissipate the response. Finally, for large initial energies, passive targeted energy transfer occurs but the initial triggering transfers a smaller fraction of the energy. By the time the energy transfer to the nonlinear energy sink is significant the total energy has decayed to a relatively small value, so that the effect of this efficient transfer on the overall evolution of the system is less significant. Therefore the most effective passive targeted energy transfer occurs when the initial triggering of the nonlinear energy sink is accompanied by a significant transfer of energy to the nonlinear energy sink.

The efficiency of the passive targeted energy transfer can be evaluated as the initial impulse varies through the maximum energy transferred to the nonlinear energy sink, $h_{2,\max}$. As illustrated in Fig. 5, as the initial energy in the system increases, the maximum energy transferred to the nonlinear energy sink undergoes a sharp jump. In this figure this quantity is shown for several values of the damping ratio ζ_2. In particular, we note that the observed jump in the transferred energy even occurs in the absence of damping, shown as the

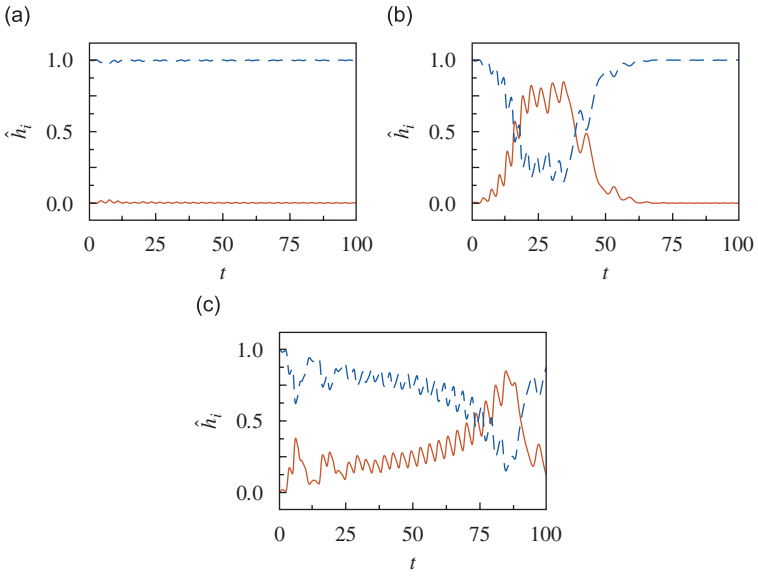

Fig. 4. Instantaneous fraction of energy in each component, nonlinear energy sink: solid line, LO: dashed line ($\alpha = 1$, $\varepsilon = 0.05$, $\zeta_1 = 0.00$, $\zeta_2 = 0.10$); (a) $Y = 0.375$, (b) $Y = 0.50$, (c) $Y = 1.00$.

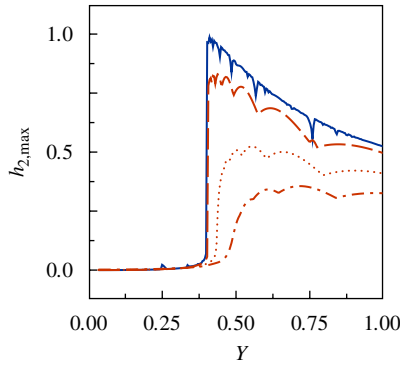

Fig. 5. Maximum energy transferred to the nonlinear energy sink ($\alpha = 1$, $\varepsilon = 0.05$, $\zeta_1 = 0.00$). Each curve corresponds to the damping in the primary with $\zeta_2 = 0.00$ ___, $\zeta_2 = 0.01$ _ _, $\zeta_2 = 0.05$ ....., $\zeta_2 = 0.10$ _ _ _ _.

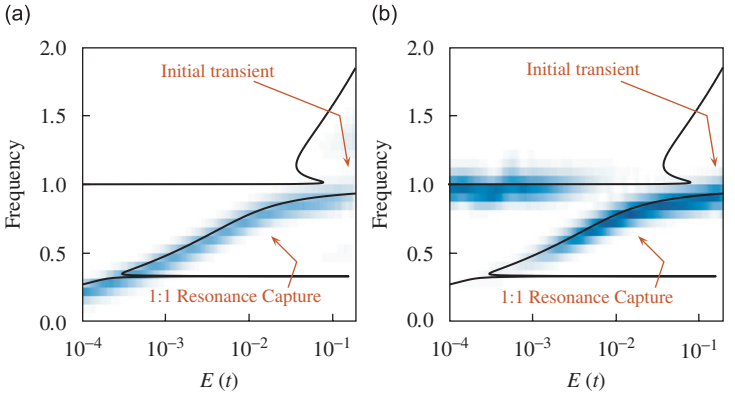

Fig. 6. Damped transitions in the frequency-energy plane for the moderate-energy regime of Fig. 3 ($Y = 0.75$, $\alpha = 1$, $\varepsilon = 0.05$, $\zeta_1 = 0.00$, $\zeta_2 = 0.01$):(a) nonlinear energy sink and (b) LO.

solid line. Therefore, the properties of the irreversible energy transfer and dissipation are strongly dependent on the dynamics of the underlying Hamiltonian system in the absence of damping.

In Refs. [3,4], the transient dynamics of the weakly damped system was studied and interpreted in terms of a frequency-energy plane by comparing the response of the damped system to that of the underlying Hamiltonian system. Such a representation is given in Fig. 6 for the moderate-energy regime of Fig. 3. In each panel the solid curve represents the frequency of the periodic solutions in the underlying Hamiltonian system, while the shading denotes the relative amplitude of the dominant harmonic components of the damped motions, as computed through the Morlet wavelet transform. The plot clearly shows the correspondence of the response of the damped system with that of the system in the absence of damping. In addition, this frequency-energy plot clearly illustrates three regimes of motion—the initial transient, followed by the 1:1 resonant motion as the initial energy decays, so that the dominant frequency of the nonlinear energy sink and LO are identical. Finally as the energy decreases near 10^{-3}, this resonant state is lost, and the frequency of the LO once again approaches unity, while that of the nonlinear energy sink remains low.

2. Slow flow

Analysis of the above system proceeds through the development of a reduced model via the method of averaging. Thus, to this system the following transformations are applied:

$$y_1(t) = a_1\cos(t+\theta_1(t)), \quad y_2(t) = a_2\cos(t+\theta_2(t)),$$
$$\dot{y}_1(t) = -a_1\sin(t+\theta_1(t)), \quad \dot{y}_2(t) = -a_2\sin(t+\theta_2(t)). \tag{3}$$

If a 1:1 resonance exists between y_1 and y_2 the difference between the phase variables, $\theta_1 - \theta_2 \equiv \phi$, is, on average, stationary. In contrast, non-resonant dynamics imply that ϕ is time-like. The resulting equations are not in the correct form for the proper application of the method of averaging. However, the polar equations are nonetheless formally averaged over $t \in [0, 2\pi)$ while holding θ_1 and θ_2 constant, which reduces these equations to

$$\dot{a}_1 = -\varepsilon\left\{\zeta_1 a_1 + \zeta_2(a_1 - a_2\cos\phi) + \frac{\alpha}{2}(a_1^2 + a_2^2 - 2a_1a_2\cos\phi)a_2\sin\phi\right\}, \tag{4a}$$

$$\dot{a}_2 = -\left\{\zeta_2(a_2 - a_1\cos\phi) - \frac{\alpha}{2}(a_1^2 + a_2^2 - 2a_1a_2\cos\phi)a_1\sin\phi\right\}, \tag{4b}$$

$$\dot{\phi} = \frac{1}{2} - \frac{\alpha}{2}(a_1^2 + a_2^2 - 2a_1a_2\cos\phi)\left[\left(1 - \frac{a_1}{a_2}\cos\phi\right) - \varepsilon\left(1 - \frac{a_2}{a_1}\cos\phi\right)\right] - \zeta_2\left(\frac{a_1}{a_2} + \varepsilon\frac{a_2}{a_1}\right)\sin\phi. \tag{4c}$$

The response of these averaged equations are later compared to the response of the original equations of motion to verify the predictions. Note that for $\zeta_1 = \zeta_2 = 0$, the following conserved quantities can be

identified:

$$a_1^2 + (\sqrt{\varepsilon}a_2)^2 \equiv r^2, \tag{5a}$$

$$\frac{a_1^2}{2} + \varepsilon\frac{a_2^2}{4} + \frac{\varepsilon\alpha}{8}(a_1^2 + a_2^2 - 2a_1a_2\cos\phi)^2 \equiv h \tag{5b}$$

and the undamped system is integrable. Taking advantage of the first of the above integrals, the phase-like variable ψ can be identified as

$$\tan\left(\frac{\psi}{2} + \frac{\pi}{4}\right) = \frac{a_1}{\sqrt{\varepsilon}a_2}, \quad \psi \in \left[-\frac{\pi}{2}, \frac{\pi}{2}\right]. \tag{6}$$

With this, the equations for $\dot{r}$ and $\dot{\psi}$ become

$$\dot{r} = \frac{a_1\dot{a}_1 + \varepsilon a_2\dot{a}_2}{r}, \quad \dot{\psi} = \frac{2\sqrt{\varepsilon}}{r^2}(\dot{a}_1a_2 - a_1\dot{a}_2), \tag{7}$$

so that the equations of motion in terms of these new variables become

$$\dot{r} = -\frac{r}{2}\{\varepsilon\zeta_1(1 + \sin\psi) + \zeta_2[(1 + \varepsilon) - (1 - \varepsilon)\sin\psi - 2\sqrt{\varepsilon}\cos\psi\cos\phi]\}, \tag{8a}$$

$$\begin{aligned}\dot{\psi} = & -\frac{\alpha r^2}{2\sqrt{\varepsilon}}[(1 + \varepsilon) - (1 - \varepsilon)\sin\psi - 2\sqrt{\varepsilon}\cos\psi\cos\phi]\sin\phi \\ & - \varepsilon\zeta_1\cos\psi + \zeta_2[(1 - \varepsilon)\cos\psi - 2\sqrt{\varepsilon}\sin\psi\cos\phi],\end{aligned} \tag{8b}$$

$$\begin{aligned}\dot{\phi} = & \frac{1}{2} - \frac{\alpha r^2}{4\varepsilon}[(1 + \varepsilon) - (1 - \varepsilon)\sin\psi - 2\sqrt{\varepsilon}\cos\psi\cos\phi] \\ & \times\left[(1 - \varepsilon) - 2\sqrt{\varepsilon}\frac{\sin\psi\cos\phi}{\cos\psi}\right] - 2\sqrt{\varepsilon}\zeta_2\frac{\sin\phi}{\cos\psi}.\end{aligned} \tag{8c}$$

If the response is localized in the LO, so that $a_2 = 0$, the phase variable becomes $\psi = \pi/2$. In contrast, a localized response in the nonlinear attachment ($a_1 = 0$) implies that $\psi = -\pi/2$. In terms of the variables (ψ, ϕ, r), in the absence of damping r is constant, and the topology of phase space is a sphere. For non-zero damping the evolution of r is slow, so that phase space is again viewed on the sphere, with a slowly varying radius. The work of Manvitch et al. [16] develops an analytical approximation for the evolution of r, which is shown to qualitatively agree with the response of the original equations of motion.

In terms of these averaged coordinates, the amplitude of the relative displacement between the LO and nonlinear energy sink, $\|y_1 - y_2\|$, is

$$\begin{aligned}\|y_1(t) - y_2(t)\|^2 &= a_1^2 + a_2^2 - 2a_1a_2\cos\phi, \\ &= \frac{r^2}{2\varepsilon}\{(1 + \varepsilon) - (1 - \varepsilon)\sin\psi - 2\sqrt{\varepsilon}\cos\psi\cos\phi\},\end{aligned} \tag{11}$$

$$= \frac{r^2}{2\varepsilon}(1 + \varepsilon)(1 - A(\phi)\sin(\psi + \gamma(\phi))) \tag{12}$$

with

$$A(\phi) = \sqrt{1 - \frac{4\varepsilon\sin^2\phi}{(1 + \varepsilon)^2}}, \quad \tan\gamma(\phi) = \frac{2\sqrt{\varepsilon}\cos\phi}{1 - \varepsilon}. \tag{13}$$

The use of the essentially nonlinear oscillator as an absorber implies that energy is initially localized in the LO and then transferred to the nonlinear attachment. As shown by Lee et al. [3], this specific situation implies that the system begins with the initial condition $a_2(0) = 0$, or in terms of the spherical coordinates, $\psi(0) = \pi/2$. The response of the damped system can be represented by two distinct phases of motion. The first corresponds to a transient response by which the system rapidly approaches a nonlinear normal mode, after which the second interval corresponds to the damped response of this nonlinear normal mode.

3. Undamped system ($\zeta_1 = \zeta_2 \equiv 0$)

As described above, in the absence of damping, that is, with $\zeta_1 = \zeta_2 \equiv 0$, r is stationary and the slow flow equations reduce to

$$\dot{r} = 0, \tag{11a}$$

$$\dot{\psi} = -\frac{\alpha r^2}{2\sqrt{\varepsilon}}[(1+\varepsilon) - (1-\varepsilon)\sin\psi - 2\sqrt{\varepsilon}\cos\psi\cos\phi]\sin\phi, \tag{11b}$$

$$\dot{\phi} = \frac{1}{2} - \frac{\alpha r^2}{4\varepsilon}[(1+\varepsilon) - (1-\varepsilon)\sin\psi - 2\sqrt{\varepsilon}\cos\psi\cos\phi]\left[(1-\varepsilon) - 2\sqrt{\varepsilon}\frac{\sin\psi\cos\phi}{\cos\psi}\right]. \tag{11c}$$

This resulting dynamical system on the sphere, described by (ψ, ϕ), is integrable, with the second integral of motion, Eq. (5b), represented as

$$\frac{r^2}{8}\left\{3 + \sin\psi + \frac{\alpha r^2}{4\varepsilon}((1+\varepsilon) - (1-\varepsilon)\sin\psi - 2\sqrt{\varepsilon}\cos\psi\cos\phi)^2\right\} = h. \tag{12}$$

Therefore, for the undamped system, trajectories in the space (ψ, ϕ) lie on level sets of this integral of motion.

Several representative phase portraits for this system are shown in Fig. 8 as the quantity r varies, which serves as the bifurcation parameter. As described in Fig. 7, these figures project the spherical topology of phase space onto the unit disk, so that the North pole at $\psi = \pi/2$ lies at the center of the disk, while the South pole ($\psi = -\pi/2$) is mapped to the unit circle. In this projection, trajectories that pass through the South pole approach the unit circle at $\phi = \pi/2$ and are continued at $\phi = -\pi/2$.

Equilibrium points are defined by $\sin\phi_{eq} = 0$, so that $\phi_{eq} = 0$ or π, and

$$\cos\psi_{eq} - \frac{\alpha r^2}{2\varepsilon}(1+\varepsilon)^2(1 - \sin(\psi_{eq} + \gamma_{eq}))\cos(\psi_{eq} + \gamma_{eq}) = 0 \tag{13}$$

with

$$\tan\gamma_{eq} = \frac{2\sqrt{\varepsilon}\cos\phi_{eq}}{1-\varepsilon}. \tag{14}$$

In general, equilibrium points for which $\phi_{eq} = 0$ correspond to an in-phase motion and have been denoted as $S11+$ by Kerschen et al. [4]. For $\phi_{eq} = \pi$ the equilibrium point represents an out-of-phase motion in the original dynamical system, denoted as $S11-$. In the projection of phase space shown in Fig. 8, $S11+$ equilibrium points with $\phi = 0$ lie on the horizontal axis to the right of the origin. Likewise, $S11-$ lies on the horizontal axis to the left of the origin ($\phi = \pi$).

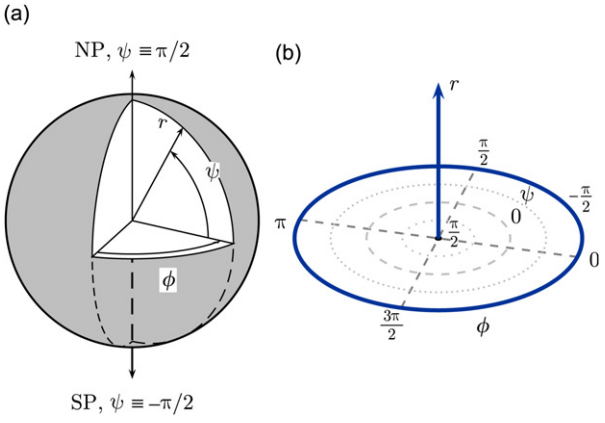

Fig. 7. Topology and representation of phase space: (a) spherical coordinates and (b) cylindrical projection.

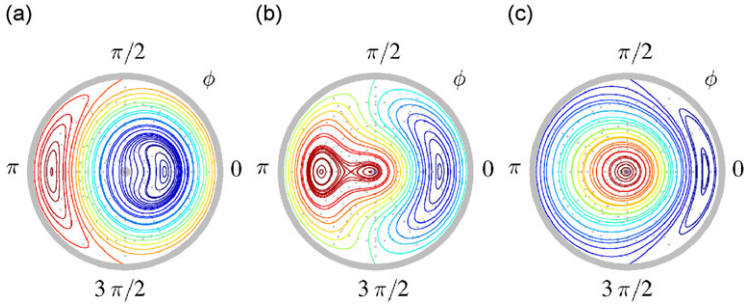

Fig. 8. Phase space projection ($\alpha = 1.00$: $\varepsilon = 0.10$); (a) $r = 1.00$, (b) $r = 0.375$ and, (c) $r = 0.25$.

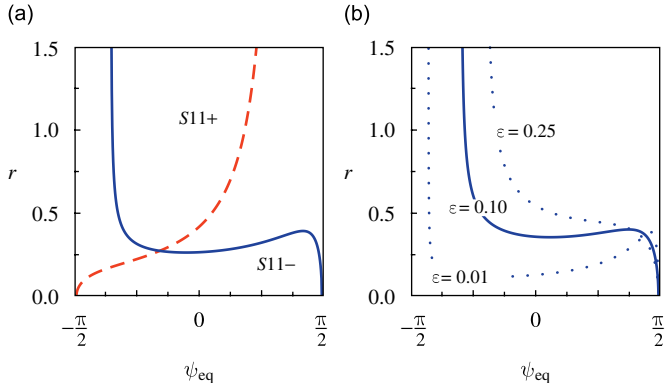

Fig. 9. Equilibrium locations ($\alpha = 1.00$): (a) $S11+$ is shown as the dashed curve while $S11-$ is shown as the solid curve ($\varepsilon = 0.05$) and (b) $S11-$ branch as ε varies.

As the value of r varies, the equilibrium values of ψ_{eq} are shown in Fig. 9a with $\alpha = 1.00$ and $\varepsilon = 0.10$. For sufficiently large values of r, phase space possesses two equilibrium points with neutral stability, one at $\phi_{eq} = 0$ and the second with $\phi_{eq} = \pi$, corresponding to $S11+$ and $S11-$, respectively. As $r \to \infty$, these equilibrium points approach a value

$$\psi_{eq} \to \arctan\left(\frac{1-\varepsilon}{2\sqrt{\varepsilon}\cos\phi_{eq}}\right), \tag{15}$$

so that for $\varepsilon < 1$, $\psi_{eq,S11+} > 0$ and $\psi_{eq,S11-} < 0$. Therefore as the energy increases the in-phase motion $S11+$ is localized to the LO, while the out-of-phase motion $S11-$ is localized to the nonlinear attachment. The degree to which this localization takes place is controlled by the mass ratio ε, and the oscillations are concentrated in a single component as $\varepsilon \to 0$.

For sufficiently small values of r the equilibrium equation for ψ_{eq} approaches

$$\cos\psi_{eq} \to 0, \quad \psi_{eq} \to \pm\frac{\pi}{2}. \tag{16}$$

Moreover, one can show that, for $S11+$, equilibrium points cannot exist in the interval $(\pi/2 - \gamma_{eq}, \pi/2)$, and, for $S11-$, equilibrium points cannot exist in the interval $(-\pi/2, -\pi/2 + |\gamma_{eq}|)$. Therefore as $r \to 0$

$$\psi_{eq,S11+} \to -\frac{\pi}{2}, \quad \psi_{eq,S11-} \to \frac{\pi}{2}. \tag{17}$$

The in-phase motion $S11+$ becomes localized to the nonlinear oscillator while the out-of-phase motion $S11-$ is localized to the LO. However, unlike the response as $r \to \infty$ described above, as $r \to 0$ the localization is complete in either the LO or nonlinear energy sink.

For an intermediate level of r with $\varepsilon = 0.05$, the $S11-$ branch undergoes a pair of saddle-node bifurcations. For decreasing r the first bifurcation occurs at $r \sim 0.40$, and a pair of equilibrium points are created near $\psi = \pi/2$. As the energy is further decreased a second saddle-node bifurcation occurs at $r \sim 0.35$, and near $\psi = 0.00$ the unstable equilibrium created in the previous bifurcation is annihilated with the branch of $S11-$ that existed for higher energies. In Fig. 9b, the $S11-$ branch of equilibria is shown as the mass ratio ε varies. A pair of saddle-node bifurcations occur in this branch for $\varepsilon < 0.171$ while for ε greater than this value the equilibrium point corresponding to an out-of-phase state is unique. In contrast, the $S11+$ branch (not shown in the figure) does not undergo saddle-node bifurcation as r varies.

3.1. Impulsive orbits

When the initial energy in the system is localized to the LO, the transient phase of the response corresponds to a trajectory with initial condition $\psi(0) = \pi/2$. In terms of the spherical topology of phase space this corresponds to a trajectory that initially lies at the North pole, and is referred to as an *impulsive orbit*. In Fig. 10 these impulsive orbits are shown as the quantity r varies. These figures also show the corresponding trajectory passing through the South pole ($\psi(0) = -\pi/2$). Finally, in Figs. 10c and d $S11-$ a third isolated trajectory is seen which lies at the same energy level as the trajectory passing through the North pole. In what follows the subscript NP will refer to the impulsive orbit passing through the North pole while subscripts SP refer to the trajectory passing through the South pole in phase space. Together, these trajectories are referred to as *pole trajectories*.

In Fig. 10 two energy levels can be identified with bifurcations of the impulsive orbit. The first, at $r \sim 0.45$ (occurring between Figs. 10g and h), corresponds to the impulsive orbit passing through both the North and South poles. For this energy level, the energy is periodically transferred completely from the LO to the

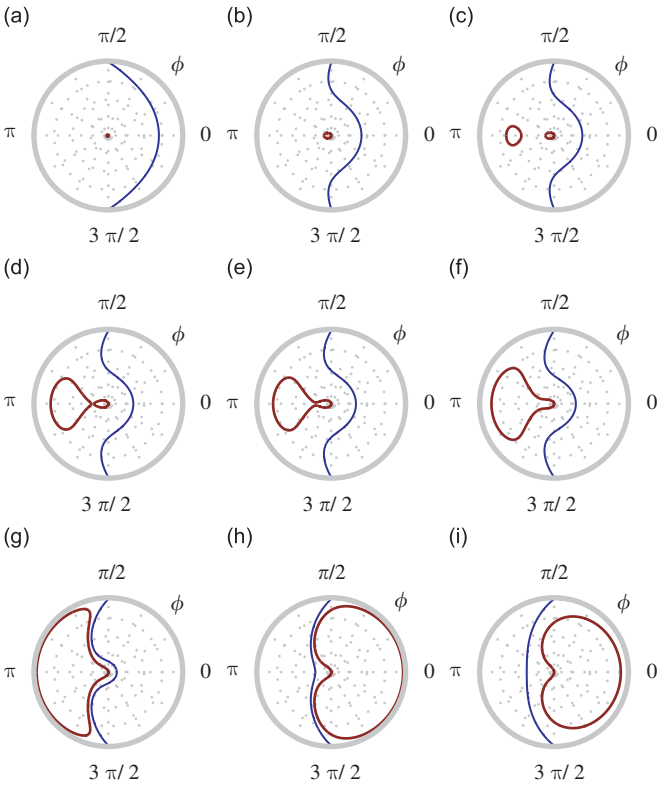

Fig. 10. Pole trajectories ($\alpha = 1.00$, $\varepsilon = 0.10$). The impulsive orbit ($\psi(0) = \pi/2$, thick line) passes through the North pole, located at the origin in this projection, while the trajectory initially localized in the nonlinear energy sink ($\psi(0) = -\pi/2$, thin line) passes through the South pole: (a) $r = 0.25$, (b) $r = 0.36$, (c) $r = 0.37$, (d) $r = 0.386$, (e) $r = 0.387$, (f) $r = 0.40$, (g) $r = 0.44$, (h) $r = 0.46$, and (i) $r = 0.50$.

nonlinear energy sink. However, the period of this orbit is finite, and the fraction of energy exchanged varies continuously as r varies, reaching a maximum value at this point. (In this case the shift in the impulsive orbit from the left to the right is an artifact of the projection.) In contrast, for a lower energy level, $r\sim0.3865$, the impulsive orbit is coincident with a homoclinic connection in phase space. While the energy is not completely exchanged in this case, as r passes through this critical value the fraction of energy continuously exchanged between the LO and nonlinear energy sink is discontinuous—the impulsive orbit transitions from low- to high-amplitude motion and enhances the energy pumping in the transient phase.

In the damped system the energy dissipation during the transient phase is related to the amplitude $\|\psi_{\mathrm{NP}}\| \equiv |\pi/2 - \psi_{\mathrm{NP}}|$ of the impulsive orbits. Further, this amplitude is related to the dynamics of the undamped system. In Fig. 11 the amplitude of the impulsive orbit in the undamped system is shown as a function of r for different values of ε. In Figs. 11a–c this amplitude undergoes a jump as r varies. Viewed in phase space, this discontinuity occurs when the impulsive orbit is coincident with the homoclinic orbit of the unstable $S11-$ equilibrium point. At this point, the period of the impulsive orbit is infinite. Note that, as shown previously, the $S11-$ branch undergoes no saddle-node bifurcations for $\varepsilon = 0.25$ so that the homoclinic orbit does not exist as r varies. As a result, the amplitude shown in Fig. 11d is continuous in r. In Figs. 11c and d there also exists a value of r for which the amplitude $\|\psi_{\mathrm{NP}}\| = \pi$. At this value of r the energy is completely exchanged between the LO and nonlinear energy sink. As described above, for this value of r the impulsive orbit passes through both the North and South poles.

The jump in the amplitude can be understood in terms of the total energy h of the impulsive orbit in relation to that of the unstable $S11-$ equilibrium point and, hence, the homoclinic orbit associated with this point. Likewise, the location at which the amplitude is maximal is related to the energy of the impulsive orbit and the trajectory passing through the South pole. The energy of the impulsive orbit is simply

$$h_{\mathrm{NP}} = \frac{r^2}{2} + \frac{\varepsilon\alpha r^4}{8}, \tag{18}$$

while the energy of the trajectory passing through the South pole is

$$h_{\mathrm{SP}} = \frac{r^2}{4} + \frac{\alpha r^4}{8\varepsilon}. \tag{19}$$

As seen in Fig. 10, the extrema of trajectories passing through the North and South poles occurs for either $\phi_{\mathrm{eq}} = 0$ or $\phi_{\mathrm{eq}} = \pi$. Therefore, from the above expressions for h_{NP} and h_{SP} the values of $\psi_\bullet$ at these energy

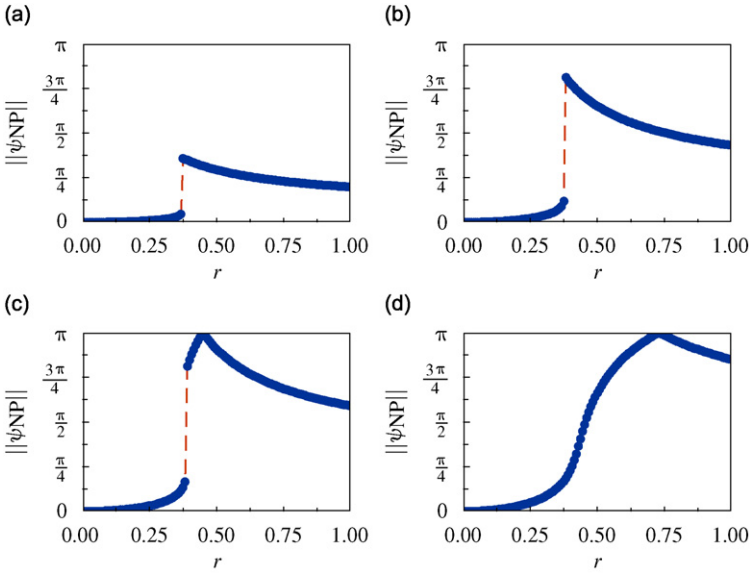

Fig. 11. Amplitude of the impulsive orbit as r varies ($\alpha = 1.00$): (a) $\varepsilon = 0.01$, (b) $\varepsilon = 0.05$, (c) $\varepsilon = 0.10$, and (d) $\varepsilon = 0.25$.

levels satisfy

$$\text{NP: } \frac{r^2}{8}(4+\varepsilon\alpha r^2) = \frac{r^2}{8}\left[3+\sin\psi_{\text{NP}} + \frac{\alpha r^2}{4\varepsilon}(1+\varepsilon)^2(1-\sin(\psi_{\text{NP}}+\gamma_{\text{eq}}))^2\right], \tag{20a}$$

$$\text{SP: } \frac{r^2}{8}\left(2+\frac{\alpha r^2}{\varepsilon}\right) = \frac{r^2}{8}\left[3+\sin\psi_{\text{SP}} + \frac{\alpha r^2}{4\varepsilon}(1+\varepsilon)^2(1-\sin(\psi_{\text{SP}}+\gamma_{\text{eq}}))^2\right] \tag{20b}$$

with

$$\tan\gamma_{\text{eq}} = \frac{2\sqrt{\varepsilon}\cos\phi_{\text{eq}}}{1-\varepsilon}. \tag{21}$$

The solutions to these equations are determined using a numerical root-finding continuation method and are shown in Fig. 12 as the mass ratio ε varies. The thin curve represents the branch ψ_{SP} while the thicker curve corresponds to the impulsive orbit ψ_{NP}. Note that there always exists a branch of ψ_{NP} at $\pi/2$ while a branch of ψ_{SP} always lies at $-\pi/2$. In these figures the dashed intervals indicate solutions of ψ for $\phi=0$ while the solid intervals of each branch correspond to $\phi=\pi$. Therefore the energy level h of the North and South poles coincide only for intersections of the branches ψ_{NP} and ψ_{SP} in Fig. 12 that occur between curves of the same linestyle (solid or dashed). These two energies are equal for

$$\alpha r^2 = 2\varepsilon/(1-\varepsilon^2). \tag{22}$$

In Fig. 12 the amplitude of the impulsive orbit $\|\psi_{\text{NP}}\|$ is measured as the distance from the North pole ($\psi=\pi/2$). For $\varepsilon=0.25$, shown in Fig. 12d, as r increases this amplitude simply increases continuously to a value of π along the solid red curve before decreasing with further increases in r along the dashed interval of ψ_{NP}. As expected, this is in complete agreement with the results shown in Fig. 10 obtained by numerical integration of the equations of motion.

As the mass ratio is decreased to $\varepsilon=0.10$, the ψ_{NP} branch contains two turning points, one of which corresponds to the coincidence of the impulsive orbit and the homoclinic orbit of the unstable $S11-$ solution described above. For $\varepsilon=0.10$ as r increases through this turning point the value of ψ_{NP} jumps to the lower solution, increases to π and then decreases along the dashed interval of ψ_{NP}, as shown in Fig. 12c. However, as the mass ratio is further decreased, as seen in Fig. 12a for $\varepsilon=0.05$, as r increases and the impulsive orbit passes through the turning point, the value of ψ_{NP} jumps directly to the dashed interval and subsequently decreases with increasing r. Specifically,

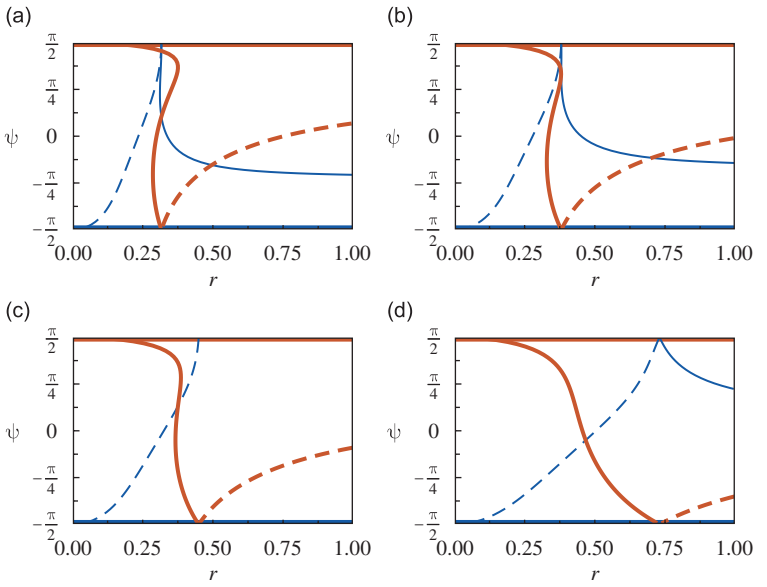

Fig. 12. Extent of the pole trajectories as r varies ($\alpha=1.00$). The amplitude of ψ_{NP} is shown with the thick line while ψ_{SP} is shown with the thin curve. For the dashed (solid) intervals $\phi=0$ ($\phi=\pi$) in Eq. (21): (a) $\varepsilon=0.05$, (b) $\varepsilon=0.072$, (c) $\varepsilon=0.10$, and (d) $\varepsilon=0.25$.

complete energy transfer, identified with $\|\psi_{NP}\| = \pi$, never occurs as r varies. For this observed behavior, as r increases the trajectory through the South pole coincides with energy level of the impulsive orbit but is not coincident with the impulsive orbit itself, which occurs before the turning point of ψ_{NP} is reached. This progression is illustrated in Fig. 13. The critical mass ratio between these two behaviors, illustrated in Figs. 12a and c, is $\varepsilon \sim 0.072$, shown in Fig. 12b. At this mass ratio the ψ_{NP} and ψ_{SP} intersect exactly at the turning point. Thus, as r increases, the amplitude of the impulsive orbit jumps to $\|\psi_{NP}\| = \pi$; that is, complete energy transfer.

In summary, the amplitude of the impulsive orbit, that is, the trajectory initially localized to the LO, depends critically on the mass ratio ε. Specifically,

(1) For ε sufficiently large the amplitude of the impulsive orbit is a continuous function of r and exhibits complete energy transfer for

$$\alpha r^2 = \frac{2\varepsilon}{1-\varepsilon^2}. \tag{23}$$

(2) As ε decreases the amplitude of the impulsive orbit becomes a discontinuous function of r. The jump occurs as the impulsive orbit coincides with a homoclinic connection created by a saddle-node bifurcation in the equilibrium states. Therefore the existence of a homoclinic connection is a necessary requirement for the observed jump in $\|\psi_{NP}\|$, although not a sufficient condition—the impulsive orbit must coincide with the homoclinic connection for some value of r. However, for intermediate values of ε the impulsive orbit still exhibits complete energy transfer for the value of r identified above.

(3) For sufficiently small mass ratios the amplitude of the impulsive orbit remains discontinuous in r, but is no longer allowed to completely exchange energy between the LO and nonlinear energy sink for any value of r. Hence, the ability of the nonlinear energy sink to passively transfer energy from the LO is expected to diminish in this regime.

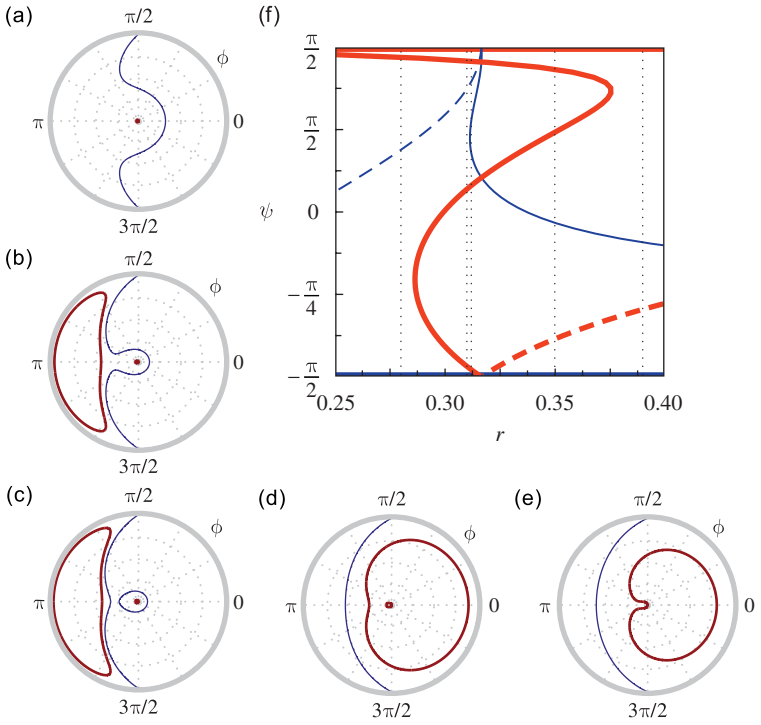

Fig. 13. Amplitude of the impulsive orbit as r varies ($\alpha = 1.00$, $\varepsilon = 0.05$); (a–e) phase space, see Fig. 10 caption for description: (a) $r = 0.28$, (b) $r = 0.31$, (c) $r = 0.312$, (d) $r = 0.35$, (e) $r = 0.39$, (f) extent of the pole trajectories (see Fig. 12 caption for linestyle description).

4. Damped system ($\zeta_1 \neq 0$, $\zeta_2 \neq 0$)

The response of the undamped system and the analysis presented above can be used as a framework for understanding the response of the system in the presence of damping. Although with ζ_1 and/or ζ_2 non-zero the trajectories are no longer constrained to integral curves ($r =$ constant, $h =$ constant) in phase space, the timescale associated with the response along integral curves is much smaller than that associated with the evolution of r and h, which is $\mathcal{O}(\varepsilon)$. Therefore, for $\mathcal{O}(1)$ durations in time, the response approximately follows an integral curve and is, therefore, qualitatively similar to the response of the undamped system. However this description breaks down in the neighborhood of a bifurcation in the undamped system, and as the energy of the system decreases the damped response will undergo qualitative changes in its response near these states.

4.1. Numerical investigation

In Fig. 14 the damped response of an impulsive orbit is shown for three different initial energy levels. Note that these can be compared to the phase portraits shown in Fig. 8 for the undamped system. In the presence of damping the equilibrium point formerly identified with $S11+$ no longer exists. The system is structurally unstable and the family of equilibria formerly parametrized by r becomes a trajectory on which the evolution is slow, of $\mathcal{O}(\varepsilon)$. Although the equilibrium point no longer exists, this normally elliptic motion can be loosely referred to as $S11+$.

For energies that are sufficiently large, shown in Fig. 14a, the response initially approaches $S11+$. This initial transient interval is followed by the slow evolution of $S11+$ as the energy decreases. Finally, the state identified with $S11+$ becomes unstable and the response localizes to the LO, so that $\lim_{t\to\infty}\psi(t) = \pi/2$. In the figure this final stage is seen as the spiraling of the trajectory toward the origin.

For lower initial energy levels, as seen in Fig. 14b, the amplitude of the fluctuations in the initial transient interval is increased. However, as for larger energy levels the response approaches $S11+$ before finally localizing to the LO as the energy becomes sufficiently small. Finally, if the initial value of r is sufficiently small, the response quickly localizes in the LO as shown in Fig. 14c, and does not approach $S11+$. Instead, the response spirals toward the origin as time increases.

In Fig. 15 the response of the system is shown versus time as obtained from numerical simulation. The total energy $h(t)$ is shown, along with $\psi(t)$ and the evolution of $\dot{h}(t)$, which describes the instantaneous change in the energy of the averaged equations, and can be written as

$$\begin{aligned}\dot{h} = & -\frac{\varepsilon\zeta_1}{2}r^2\left\{1+\sin\psi+\frac{\alpha r^2}{4}(\varepsilon(1+\sin\phi)-\sqrt{\varepsilon}\cos\psi\cos\phi)[(1+\varepsilon)\right.\\ & \left.-(1-\varepsilon)\sin\psi-2\sqrt{\varepsilon}\cos\psi\cos\phi]\right\}-\frac{\zeta_2}{4}r^2[(1+\varepsilon)-(1-\varepsilon)\sin\psi\\ & -2\sqrt{\varepsilon}\cos\psi\cos\phi]\left\{1+\frac{\alpha r^2}{2\varepsilon}(1+\varepsilon)[(1+\varepsilon)-(1-\varepsilon)\sin\psi\right.\\ & \left.-2\sqrt{\varepsilon}\cos\psi\cos\phi]\right\}. \end{aligned} \tag{24}$$

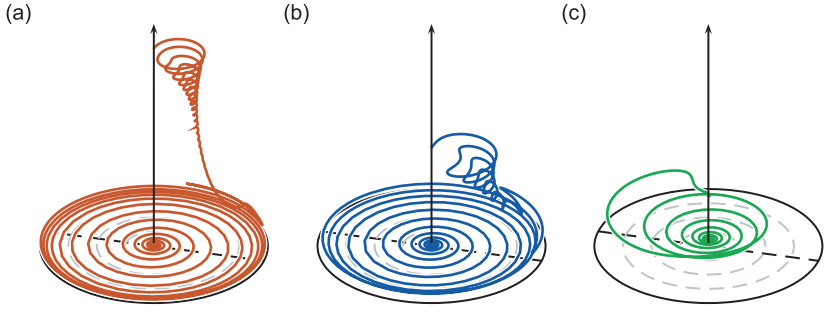

Fig. 14. Phase space projection ($\alpha = 1.00$, $\varepsilon = 0.10$, $\zeta_1 = \zeta_2 = 0.05$): (a) $r(0) = 2.00$, (b) $r(0) = 1.00$, and (c) $r(0) = 0.50$.

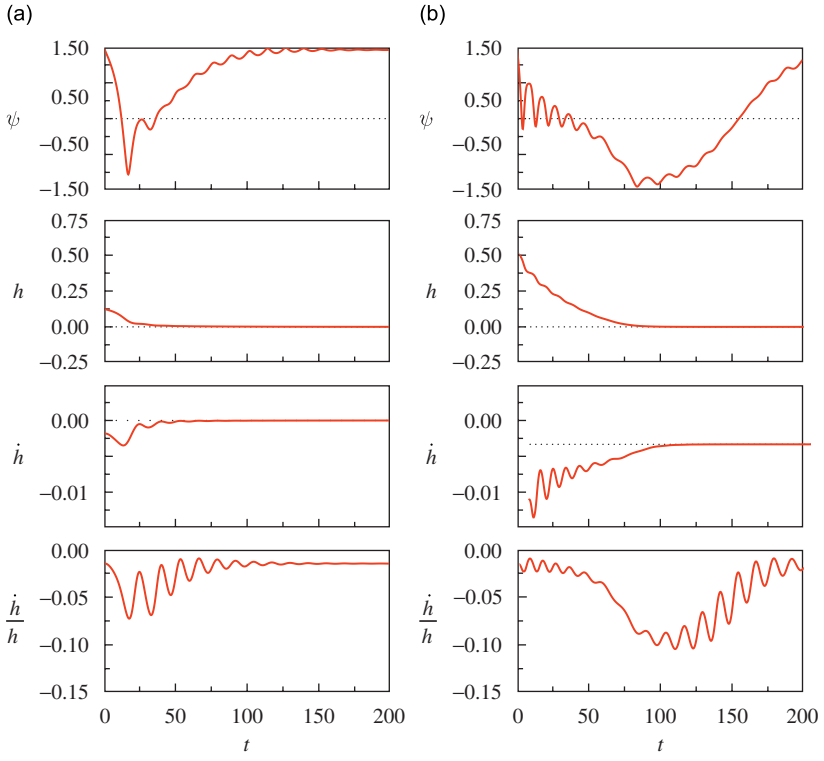

Fig. 15. Numerical integration of the impulsive orbit ($\varepsilon = 0.10$, $\alpha = 1.00$, $\zeta = 0.05$): (a) $r(0) = 0.50$ and (b) $r(0) = 1.00$.

The above equation on $\dot{h}$ is not considered as part of the equations of motion, although it could in principle replace one of the equations in Eqs. (8). Instead, the response of $r(t)$, $\psi(t)$, and $\phi(t)$ are determined numerically and then $\dot{h}(t)$ is calculated *a posteriori*. Finally, the quantity $\dot{h}(t)/h(t)$, which represents the instantaneous exponential decay rate of the energy, is also shown.

The instantaneous power dissipated in the nonlinear energy sink, defined as P_{NES} can be determined from (24) with $\zeta_1 \equiv 0$, and the nonlinear energy sink is most effective when the power is maximal. In Fig. 16 the level sets of P_{NES} are constructed in phase space for fixed r. These equi-power curves coincide with the level sets of the amplitude of $\|y_1 - y_2\|$ (see Eq. (9)), equivalent to curves in phase space for which

$$\begin{aligned}&(1+\varepsilon) - (1-\varepsilon)\sin\psi - 2\sqrt{\varepsilon}\cos\psi\cos\phi\\ &\quad = (1+\varepsilon)(1 - A(\phi)\sin(\psi + \gamma(\phi))) = \text{constant}.\end{aligned} \tag{25}$$

Note that this quantity is independent of r. Although r changes the value of P_{NES}, it does not affect the geometry of the level sets of this quantity.

As a function viewed in phase space, the power dissipated in the nonlinear energy sink possesses two extrema, seen as stationary points in Fig. 16. The stationary point that lies along the curve $\phi = 0$ (to the right of the origin) is a minimum, while the point for $\phi = \pi$ is a maximum. These stationary points do not coincide with the equilibria $S11\pm$, although as $r \to \infty$ the equilibria $S11\pm$ approach these stationary points. From Fig. 16, the most efficient energy dissipation occurs for trajectories that are located away from the minimum of P_{NES}, located at

$$\psi = \frac{\pi}{2} - \gamma(0) = \frac{\pi}{2} - \arctan\left(\frac{2\sqrt{\varepsilon}}{1-\varepsilon}\right), \tag{26}$$

which lies near $S11+$. In contrast, the maximum of P_{NES} occurs at $\psi = -\pi/2 + \gamma(0)$.

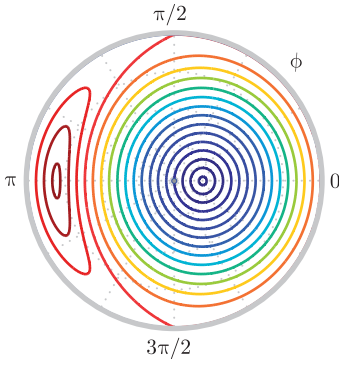

Fig. 16. Level sets of P_{NES} ($\varepsilon = 0.10$).

Revisiting the numerical simulations shown in Fig. 14, the trajectories shown in Figs. 14a and b with $r(0) = 2.00$ and $r(0) = 1.00$, respectively, are quickly drawn toward $S11+$ and into a region of inefficient dissipation. As the energy is further decreased the trajectory follows $S11+$ and the rate of energy loss is expected to slowly increase with this drift. In contrast, the trajectory for $r(0) = 0.50$ undergoes an initial interval of motion that takes it into a region of efficient dissipation as seen in Fig. 16. Thus the energy loss induced by the nonlinear energy sink is expected to be significant in these initial motions.

These conjectures are verified in Fig. 15. In each simulation the initial transient motion is accompanied by a relatively large decrease in the total energy. As the response approaches $S11+$ the rate of the energy decrease is reduced. Recall that $S11+$ is an in-phase motion so that the relative displacement between the masses, and hence the effect of the coupling including the damping ζ_2 is small. In contrast, during the initial transient motion the relative displacement is larger, as is the associated dissipation. Note however that the exponential decay rate $\dot{h}(t)/h(t)$ is largest when $S11+$ loses stability and the system moves toward a response localized in the LO. This implies that the energy dissipation is most efficient during this transition between $S11+$ and $S11-$, when the trajectories move through a region of enhanced dissipation.

The most effective energy dissipation occurs when the efficient response described above occurs for relatively large energies. As illustrated in Fig. 15a, with $r(0) = 0.50$, the transition occurs almost immediately when the energy h is still large. In contrast, for $r(0) = 1.00$ the response is attracted to $S11+$ during the initial transient phase, but note that the exponential rate remains small. The efficient energy dissipation does not occur until $t \sim 75$, for which the energy has already decayed to a low value—the energy dissipation at this point is efficient but it is not necessarily effective. Finally, for sufficiently small initial energies, so that the impulsive orbit remains near $S11-$, the trajectory is localized to the LO, and the efficient energy dissipation described above does not occur.

The effectiveness of the nonlinear energy sink at dissipating energy from the impulsive orbits therefore depends on two factors: the first is the geometry of the impulsive orbit itself, which is approximated by that for the undamped system. The second influence arises from the effect of damping on the resulting flow through P_{NES}. Recall the qualitative behavior of the undamped system in which the impulsive orbits undergo a jump in their amplitude as the initial energy varies. This jump arises from the homoclinic connection seen in phase space in Fig. 8. For sufficiently small initial energies the amplitude of the impulsive orbit is small, and more importantly for the resulting efficiency of the nonlinear energy sink, lies within a region of limited power dissipation. Moreover, the dissipation serves to keep the resulting damped orbit within this region. As the energy increases, the amplitude of the impulsive orbit jumps, taking the impulsive orbit into a region of increased P_{NES}, and the efficiency of the nonlinear energy sink increases. With ever increasing initial energies, the impulsive orbit quickly approaches $S11+$ due to damping, which lies within a region of lower P_{NES}.

The efficiency of the nonlinear energy transfer from the impulsive orbit is described by the time required for the value of $r(t)$ to decay by a factor of $\exp(1)$ so that $r(T) = r(0)\mathrm{e}^{-1}$, which, for a linear system, is defined as the time constant. However, in the present nonlinear system this value is not strictly a property of the components and also depends on the initial conditions. Nonetheless this numerically computed value,

identified as T, is used to compare the response of the system for varying parameters and initial conditions—increased efficiency corresponds to smaller values of T.

In Fig. 17 the variation of T is shown for $\varepsilon = 0.05$, $\zeta_1 = 0.00$, and $\zeta_2 = 0.10$ as $r(0)$ varies. Here $\zeta_1 = 0.00$ was chosen to focus on the dissipation in the attachment. In addition, the impulsive orbit is shown for this time interval at several different energy levels. Near $r(0) = 0.46$ there is a sharp decrease in the numerically computed value of T. As seen in Figs. 17b and c, at this point the impulsive orbit undergoes a sudden jump in amplitude and moves from a localized response in the LO for $r(0) = 0.46$ to a larger amplitude motion that moves into a region of increased energy dissipation in the nonlinear energy sink (cf. Fig. 16).

For a linear single degree- of- freedom system with damping ratio $\varepsilon\zeta$ and unit natural frequency, the expected value of T is $\varepsilon\zeta$. In Fig. 18a the quantity $\hat{T} \equiv T/(\varepsilon\zeta_2)$ is shown as a function of ε and $r(0)$. The value of $\hat{T}$ undergoes a sharp decrease near $r(0)\sim0.45$, attributed to the geometry of the unperturbed system as illustrated in Fig. 17. Recall that decreases in T indicate increased efficiency of the energy transfer. However, this scaled decay time is relatively insensitive to the mass ratio ε. The jump in efficiency is most pronounced for small values of the mass ratio ε, for which the IO surrounds the $S11-$ state at the bifurcation. For larger mass ratios the IO of the unperturbed system surrounds $S11+$ as described in Fig. 12, and the decrease in T is more gradual.

For fixed mass ratio ε, similar conclusions can be drawn as the damping ratio ζ_2 varies. As shown in Fig. 18b, holding the damping constant, for low initial energies the value of $\hat{T}$ is relatively large and $\hat{T}$ actually increases with increasing damping, indicating that the system requires longer to decay relative to the expected value of $\varepsilon\zeta_2$ (although the actual time decreases). For fixed ζ_2 sufficiently small, as $r(0)$ increases the decay time $\hat{T}$ undergoes a sharp decrease. Note, however, that the location in $r(0)$ of this transition increases as ζ_2 increases, and the transition itself becomes more gradual. As the damping increases the geometry of the unperturbed system plays a less significant role on the evolution of the damped system. In fact, for sufficiently large damping, no significant increase in the efficiency of the energy transfer occurs.

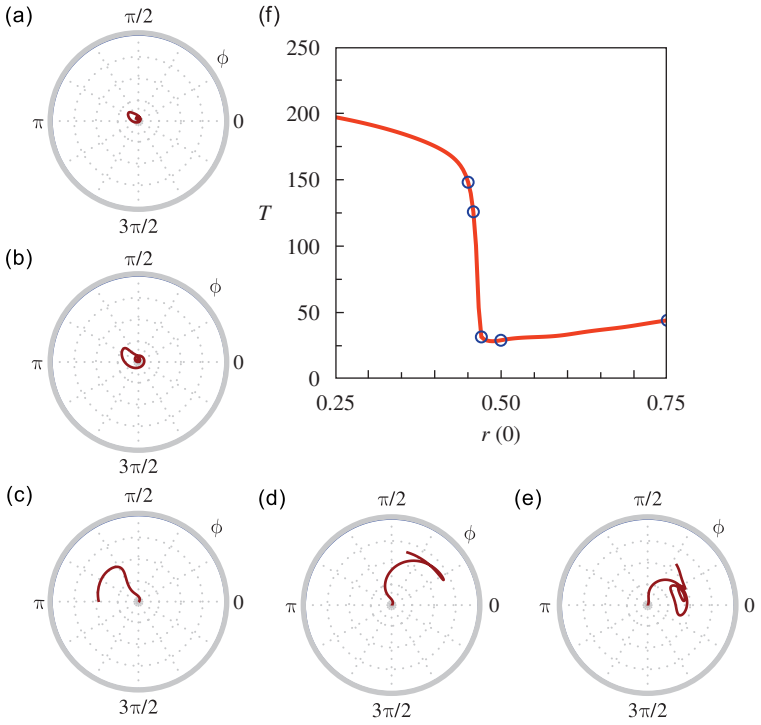

Fig. 17. Numerical simulations of impulsive orbits as $r(0)$ varies ($\alpha = 1.00$, $\varepsilon = 0.05$, $\zeta_2 = 0.10$). The points marked in (f) correspond to the phase portraits shown in (a–e): (a) $r(0) = 0.45$, (b) $r(0) = 0.46$, (c) $r(0) = 0.47$, (d) $r(0) = 0.50$, (e) $r(0) = 0.75$ and, (f) nonlinear energy sink efficiency.

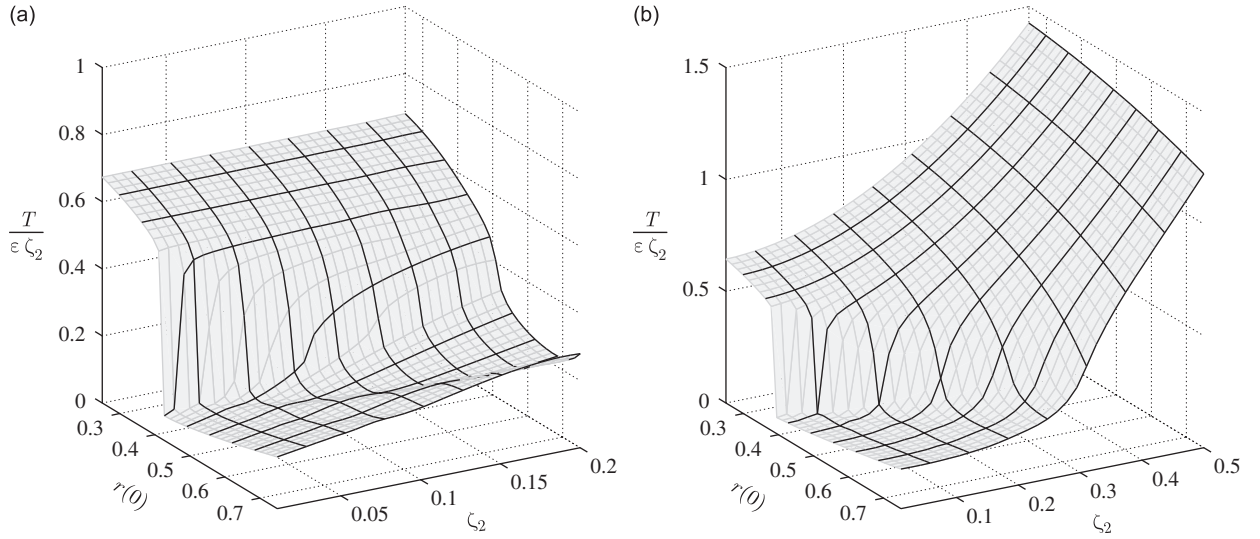

Fig. 18. Time required for the impulsive orbit to reach $r(0)/2$ ($\alpha = 1.00$, $\varepsilon, \zeta_1 = 0.00$): (a) $\zeta_2 = 0.10$, $0.01 \leqslant \varepsilon \leqslant 0.20$ and (b) $\varepsilon = 0.05$, $0.01 \leqslant \zeta_2 \leqslant 0.50$.

4.2. Stability of $S11\pm$

From the long-time behavior of the impulsive orbits shown in Figs. 14 and 15, we observe that for sufficiently large initial values of $r(0)$ the response is initially attracted to $S11+$ before transitioning to $S11-$ with the response becoming localized in the LO. During this transition the efficiency of the energy dissipation in the nonlinear energy sink is increased. This transition can be associated with a change in stability of $S11+$ in directions normal to the evolution along $S11+$.

The damped equations of motion can be formally written as

$$\dot{r} = \zeta g_r, \quad \dot{\mathbf{x}} = \mathbf{f}_{\mathbf{x}} + \zeta \mathbf{g}_{\mathbf{x}}, \quad \mathbf{x} = [\psi, \phi]^{\mathrm{T}}, \tag{27}$$

where the functions $\mathbf{f}_{\mathbf{x}}$, $\mathbf{g}_{\mathbf{x}}$, and g_r can be determined from Eq. (8a). To these equations we assume that ζ, which represents the strength of the damping, is the expansion parameter and identify the new time scale $\tau = \zeta t$. The method of multiple scales is applied to these equations, with the additional identification of the timescale introduced by r, so that

$$\frac{\mathrm{d}}{\mathrm{d}t} = \frac{\partial}{\partial t} + \zeta \frac{\partial}{\partial \tau} + \zeta\, g_r\, \frac{\partial}{\partial r} \tag{28}$$

and the state variables are expanded in ζ.

At $\mathcal{O}(\zeta^0)$ the equations of motion reduce to

$$\frac{\partial \mathbf{x}_0}{\partial t} = \mathbf{f}_{\mathbf{x}}(\mathbf{x}_0, r). \tag{29}$$

The states identified as $S11\pm$ correspond to slowly varying nonlinear normal modes of the original system and are identified as equilibrium points at this order on the fast timescale, so that

$$\mathbf{f}_{\mathbf{x}}(\mathbf{x}_0, r) = \mathbf{0}, \tag{30}$$

which can formally be solved so that $\mathbf{x}_0 = \mathbf{x}_0(r)$, that is, parametrized by r. Also, note that $\mathbf{x}_0$ is independent of the slow timescale τ. In addition, from $\mathbf{x}_0(r)$

$$\frac{\partial \mathbf{x}_0(r)}{\partial r} = -[\nabla \mathbf{f}_{\mathbf{x}}(\mathbf{x}_0, r)]^{-1} \cdot \frac{\partial \mathbf{f}_{\mathbf{x}}(\mathbf{x}_0, r)}{\partial r}. \tag{31}$$

At $\mathcal{O}(\zeta^1)$, the expansion can be reduced to

$$\frac{\partial \mathbf{x}_1}{\partial t} = \nabla \mathbf{f}_{\mathbf{x}}(\mathbf{x}_0, r) \cdot \mathbf{x}_1 + \left\{ \mathbf{g}_{\mathbf{x}}(\mathbf{x}_0, r) - g_r(\mathbf{x}_0, r) \frac{\partial \mathbf{x}_0(r)}{\partial r} \right\}. \tag{32}$$

The solution can be written in the form $\mathbf{x}_1 = \mathbf{q}_1 + \mathbf{s}_1$, with

$$\mathbf{s}_1 = -[\nabla \mathbf{f}_{\mathbf{x}}(\mathbf{x}_0, r)]^{-1} \cdot \left\{ \mathbf{g}_{\mathbf{x}}(\mathbf{x}_0, r) - g_r(\mathbf{x}_0, r)[\nabla \mathbf{f}_{\mathbf{x}}(\mathbf{x}_0, r)]^{-1} \cdot \frac{\partial \mathbf{f}_{\mathbf{x}}(\mathbf{x}_0, r)}{\partial r} \right\}, \tag{33}$$

so that

$$\frac{\partial \mathbf{q}_1}{\partial t} = \nabla \mathbf{f}_{\mathbf{x}}(\mathbf{x}_0, r) \cdot \mathbf{q}_1. \tag{34}$$

Finally, at $\mathcal{O}(\zeta^2)$

$$\begin{aligned} \frac{\partial \mathbf{x}_2}{\partial t} = {} & \nabla \mathbf{f}_{\mathbf{x}}(\mathbf{x}_0, r) \cdot \mathbf{x}_2 - \left[\frac{\partial \mathbf{q}_1}{\partial \tau} + g_r(\mathbf{x}_0, r) \frac{\partial \mathbf{q}_1}{\partial r} \right] \\ & + \left\{ \nabla \mathbf{g}_{\mathbf{x}}(\mathbf{x}_0, r) + [\nabla \mathbf{f}_{\mathbf{x}}(\mathbf{x}_0, r)]^{-1} \cdot \frac{\partial \mathbf{f}_{\mathbf{x}}(\mathbf{x}_0, r)}{\partial r} \otimes \nabla g_r(\mathbf{x}_0, r) + \nabla \nabla \mathbf{f}_{\mathbf{x}}(\mathbf{x}_0, r) \cdot \mathbf{s}_1 \right\} \cdot \mathbf{q}_1 \\ & - \left[\frac{\partial \mathbf{s}_1}{\partial \tau} + g_r(\mathbf{x}_0, r) \frac{\partial \mathbf{s}_1}{\partial r} \right] + \left\{ \nabla \mathbf{g}_{\mathbf{x}}(\mathbf{x}_0, r) + [\nabla \mathbf{f}_{\mathbf{x}}(\mathbf{x}_0, r)]^{-1} \cdot \frac{\partial \mathbf{f}_{\mathbf{x}}(\mathbf{x}_0, r)}{\partial r} \otimes \nabla g_r(\mathbf{x}_0, r) \right\} \cdot \mathbf{s}_1 \\ & + \frac{1}{2} \{ \mathbf{s}_1 \cdot \nabla \nabla \mathbf{f}_{\mathbf{x}}(\mathbf{x}_0, r) \cdot \mathbf{s}_1 + \mathbf{q}_1 \cdot \nabla \nabla \mathbf{f}_{\mathbf{x}}(\mathbf{x}_0, r) \cdot \mathbf{q}_1 \}. \end{aligned} \tag{35}$$

In this expression the terms that are linear in $\mathbf{q}_1$ contribute to the secular terms whose removal provides the slow flow equations. Specifically, if $(\lambda_i, \mathbf{u}_i)$, $i = 1, 2$, are the eigenpairs of $\nabla \mathbf{f}_{\mathbf{x}}$ then $\mathbf{q}_1$ can be written as

$$\mathbf{q}_1 = c_1(r, \tau) e^{\lambda_1 t} \mathbf{u}_1 + c_2(r, \tau) e^{\lambda_2 t} \mathbf{u}_2. \tag{36}$$

Identifying $\mathbf{v}_i$, $i = 1, 2$ as the dual basis, so that $\bar{\mathbf{v}}_i \cdot \mathbf{u}_j = \delta_{ij}$, then removal of secular terms requires that

$$\begin{aligned} \frac{\partial c_i}{\partial \tau} + g_r(\mathbf{x}_0, r) \frac{\partial c_i}{\partial r} = {} & \left\{ \bar{\mathbf{v}}_i \cdot \left[\nabla \mathbf{g}_{\mathbf{x}}(\mathbf{x}_0, r) + [\nabla \mathbf{f}_{\mathbf{x}}(\mathbf{x}_0, r)]^{-1} \cdot \frac{\partial \mathbf{f}_{\mathbf{x}}(\mathbf{x}_0, r)}{\partial r} \otimes \nabla g_r(\mathbf{x}_0, r) \right. \right. \\ & \left. \left. + \nabla \nabla \mathbf{f}_{\mathbf{x}}(\mathbf{x}_0, r) \cdot \mathbf{s}_1 \right] \cdot \mathbf{u}_i \right\} c_i. \end{aligned} \tag{37}$$

This equation can be solved with the method of characteristics, which are defined by the curves

$$\frac{\mathrm{d}r}{\mathrm{d}\tau} = g_r(\mathbf{x}_0, r), \tag{38}$$

so that along the characteristics

$$\frac{\partial c_i}{\partial \tau} + g_r(\mathbf{x}_0, r) \frac{\partial c_i}{\partial r} = \frac{\mathrm{d}c_i}{\mathrm{d}\tau}. \tag{39}$$

and the variational equation reduces to

$$\frac{\mathrm{d}c_i}{\mathrm{d}\tau} = \sigma(r) c_i, \tag{40a}$$

$$\frac{\mathrm{d}r}{\mathrm{d}\tau} = g_r(\mathbf{x}_0(r), r) \tag{40b}$$

with the exponential rate σ defined as

$$\begin{aligned} \sigma = {} & \left\{ \varepsilon \zeta_1 \sin \psi_{\mathrm{eq}}(r) - \zeta_2 (1 + \varepsilon) \left(\frac{\sin \gamma + \sin(2 \psi_{\mathrm{eq}}(r) + \gamma)}{2 \cos \psi_{\mathrm{eq}}(r)} \right) \right. \\ & \left. + \frac{\varepsilon \zeta_1 (\sin \psi_{\mathrm{eq}}(r) - \cos 2\psi_{\mathrm{eq}}(r)) + \zeta_2 (1 + \varepsilon)(\sin \psi_{\mathrm{eq}}(r) + \cos(2(\psi_{\mathrm{eq}}(r) + \gamma)))}{2 \sin \psi_{\mathrm{eq}}(r) - \frac{\alpha r^2}{\varepsilon} (1 + \varepsilon)^2 (\cos(2(\psi_{\mathrm{eq}}(r) + \gamma)) + \sin(\psi_{\mathrm{eq}}(r) + \gamma))} \right\}. \end{aligned} \tag{41}$$

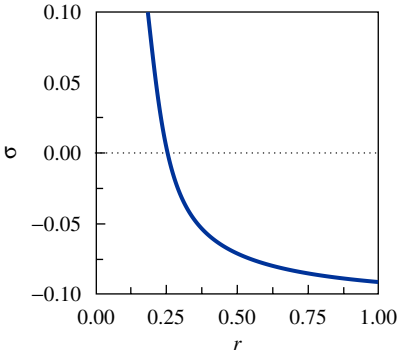

Fig. 19. Exponential rate ($\varepsilon = 0.05$, $\alpha = 1.00$, $\zeta_1 = \zeta_2 = 0.05$).

The final term in this expression arises solely from the slow evolution in r, that is, for $g_r \equiv 0$ this last term vanishes. Also note that in this equation ψ_{eq} represents the equilibrium value of ψ, which is a function of r, and r depends on the slow timescale τ through the definition of the characteristic. The evolution equation given above can be formally solved to yield

$$c_i(\tau) = c_i(0) \exp\left\{ \int_0^\tau \sigma(r(s))\, \mathrm{d}s \right\}, \tag{42}$$

where $r(\tau)$ is determined independently from $c_i(\tau)$. Therefore the growth or decay of the amplitude of solutions near $S11$ is determined by the sign of σ, which is in turn only a function of r. In Fig. 19 the exponential rate σ is shown for $S11+$ as a function of r, with $\varepsilon = 0.05$, $\alpha = 1.00$, and $\zeta_1 = \zeta_2 = 0.05$. For r sufficiently large ($r > 0.30$) $\sigma < 0$, indicating that solutions are attracted to $S11+$. However, as energy is lost in the damped system and r decreases, σ changes sign and solutions diverge from $S11+$. This progression matches the behavior illustrated in simulations of the averaged system, shown in Figs. 14 and 15.

5. Concluding remarks

The findings of this work confirm that, for sufficiently weak damping, nonlinear damped transitions are essentially influenced by the underlying Hamiltonian dynamics. It follows that significant understanding and interpretation of (even complicated and multi-frequency) damped nonlinear transitions in the dynamics can be gained by performing perturbation studies that use as generating functions the Hamiltonian periodic or quasi-periodic orbits. An additional finding in this work is the central role that impulsive orbits play on efficient targeted energy transfers passive targeted energy transfers from the (directly excited) LO to the essentially nonlinear attachment. Based on the study of impulsive orbits and under the assumption of 1:1 resonance capture, we were able to determine conditions on the system parameters and forcing level for which optimal passive targeted energy transfer occurs, e.g., conditions where a major part of the vibration energy of the LO gets passively transferred and locally dissipated by the nonlinear attachment in the least possible time. In addition to this observed localization to $S11+$, energy dissipation in the system is enhanced during the transition from $S11+$ to $S11-$. Therefore, the novel energy dissipation properties of the essentially nonlinear system arise from the localization of the slowly varying nonlinear normal modes and the transition between 1:1 resonance captures. The analytic investigation of optimal passive targeted energy transfer will be reported in a companion work, where the boundaries in parameter space separating optimal from inefficient passive targeted energy transfer will be formulated.

Acknowledgments

This material is based upon work supported by the National Science Foundation under Grant no. CMS–0201347 (DDQ). The author GK is supported by a grant from the Belgian National Science Foundation (FNRS), which is gratefully acknowledged.

References

[1] V.I. Arnold, V.V. Kozlov, A.I. Neishtadt, *Mathematical Aspects of Classical and Celestial Mechanics, Vol. 3 of Encyclopedia of Mathematical Sciences: Dynamicial Systems III*, Springer, Berlin, 1985.

[2] D.D. Quinn, Transition to escape in a system of coupled oscillators, *International Journal of Nonlinear Mechanics* 32 (6) (1997) 1193–1206.

[3] Y.S. Lee, G. Kerschen, A.F. Vakakis, P. Panagopoulos, L. Bergman, D.M. McFarland, Complicated dynamics of a linear oscillator with a light, essentially nonlinear attachment, *Physica D* 204 (1–2) (2005) 41–69.

[4] G. Kerschen, Y.S. Lee, A.F. Vakakis, D.M. McFarland, L. Bergman, Irreversible passive energy transfer in coupled oscillators with essential nonlinearity, *SIAM Journal on Applied Mathematics* 66 (2006) 648–679.

[5] A.F. Vakakis, L.I. Manevitch, O. Gendelman, L. Bergman, Dynamics of linear discrete systems connected to local, essentially nonlinear attachments, *Journal of Sound and Vibration* 264 (2003) 559–577.

[6] D.M. McFarland, L.A. Bergman, A.F. Vakakis, Experimental study of nonlinear energy pumping occurring at a single fast frequency, *International Journal of Non-Linear Mechanics* 40 (6) (2005) 891–899.

[7] G. Kopidakis, S. Aubry, G.P. Tsironis, Targeted energy transfer through discrete breathers in nonlinear systems, Physical Review Letters 87 (2001) 165501–1.

[8] S. Aubry, S. Kopidakis, A.M. Morgante, G.P. Tsironis, Analytic conditions for targeted energy transfer between nonlinear oscillators for discrete breathers, *Physica B* 296 (2001) 222–236.

[9] A.M. Morgante, M. Johansson, S. Aubry, G. Kopidakis, Breather-phonon resonances in finite-size lattices: ''Phantom breathers,'' *Journal of Physics A* 35 (2002) 4999–5021.

[10] D.L. Vainchtein, E.V. Rovinsky, L.M. Zelenyi, A.I. Neishtadt, Resonances and particle stochastization in nonhomogeneous electromagnetic fields, *Journal of Nonlinear Science* 14 (2004) 173–205.

[11] K.R. Khusnutdinova, D.E. Pelinovsky, On the exchange of energy in coupled Klein-Gordon oscillators, *Wave Motion* 38 (2003) 1–10.

[12] P. Maniadis, G. Kopidakis, S. Aubry, Classical and quantum targeted energy transfer between nonlinear oscillators, *Physica D* 188 (2004) 153–177.

[13] C.W. Cai, H.C. Chan, Y.K. Cheung, Localized modes in a two-degree-coupled periodic systems with a nonlinear disordered subsystem, *Chaos, Solitons & Fractals* 11 (2000) 1481–1492.

[14] P. Malatkar, A.H. Nayfeh, On the transfer of energy between widely spaced modes in structures, *Nonlinear Dynamics* 31 (2003) 225–242.

[15] S.J. Zhu, Y.F. Zheng, Y.M. Fu, Analysis of nonlinear dynamics of a two-degree-of-freedom vibration system with nonlinear damping and nonlinear spring, *Journal of Sound and Vibration* 271 (2004) 15–24.

[16] L.I. Manevitch, A.I. Musienko, C.-H. Lamarque, New analytical approach to energy pumping problem in strongly nonhomogeneous 2dof systems, *Meccanica* 42 (2007) 77–83.

[17] O. Gendelman, G. Kerschen, A.F. Vakakis, L. Bergman, D.M. McFarland, Impulsive periodic and quasiperiodic orbits in a system of coupled oscillators with essential stiffness nonlinearity, Communications in Nonlinear Science and Numerical Simulation, in press.